12

Molecular Beam Epitaxy of $Cd_xHg_{1-x}Te$

Yu.G. Sidorov[1], A.P. Anciferov[1], V.S. Varavin[1], S.A. Dvoretsky[1], N.N. Mikhailov[1], M.V. Yakushev[1], I.V. Sabinina[1], V.G. Remesnik[1], D.G. Ikusov[1], I.N. Uzhakov[1], G.Yu. Sidorov[1], V.D. Kuzmin[1], S.V. Rihlicky[1], V.A. Shvets[1], A.S. Mardezov[1], E.V. Spesivcev[1], A.K. Gutakovskii[1], A.V. Latyshev[1,2]

[1]RZHANOV INSTITUTE OF SEMICONDUCTOR PHYSICS OF THE SIBERIAN BRANCHOF THE RUSSIAN ACADEMY OF SCIENCES, NOVOSIBIRSK, RUSSIA [2]NOVOSIBIRSK STATE UNIVERSITY, NOVOSIBIRSK, RUSSIA

Infrared imaging systems are required for applications in medicine, agriculture, the chemical industry, ferrous and nonferrous metals metallurgy, the fuel industry, and other areas of the economy. Due to high quantum efficiency, tunable absorption wavelength, and a wide operating temperature range, HgCdTe (mercury cadmium telluride, MCT)-based infrared focal plane arrays are a good choice for the fabrication of high-performance infrared imaging systems. Creating arrays and matrices of photodetectors with a large number of elements imposes stringent requirements for narrow-band MCT. What is wanted is a large area plate MCT with highly uniform properties and low cost.

MCT technology over the past 20 years has evolved from the production of relatively small (diameter $<$10 mm) volume bars to large (up to 150 mm in diameter) epitaxial layers on alternative substrates. The electrical properties of solid solutions MCT are largely determined by the intrinsic point defects and residual impurities associated with the growing method. MCT is characterized by a high rate of diffusion of point defects. Therefore, a low growth temperature is need. These requirements are best suited to epitaxial techniques of growth. Molecular beam epitaxy (MBE) MCT technology has reached the level required for the preparation of material for practical applications. The material quality of the instrument grows with the composition of the alloys required for the application for all wavelengths;—from short-wave to a very long wavelength. In the MCT films grown by MBE, a concentration of conduction electrons (1−5) of 10^{14} cm^{-3} is routinely obtained, which is not inferior to the results obtained by liquid phase epitaxy (LPE), and developed methods of doping donor and acceptor impurities. Growth rates in the map layers using MBE currently account for 3−5 μm/h, with working layers of 10−15 μm thick grown in no more than 3 h, which is comparable to the times for growing layers using the LPE method. MBE is the most promising method for growing MCT layers on substrates of CdZnTe, gallium arsenide, and silicon. MBE is superior to other methods for growing MCT films because of a number of circumstances.

Advances in Semiconductor Nanostructures. DOI: http://dx.doi.org/10.1016/B978-0-12-810512-2.00012-3

12.1 Advantages and Problems of MBE MCT

1. MCT photodiodes with a heterojunction currently display the best characteristics. Heterostructures grown by LPE are usually limited to two or three layers, because different melts are required for the preparation of layers differing in composition and doping. MBE is ideally suitable for the growth of layers differing in composition and doping. MBE is also ideally suitable for deposition of multilayer structures used in two-color IR-videosystems and monolithic IR-arrays. MBE is the only technique well adapted to the fabrication of superlattice detectors for the very long-wave infrared range consisting of alternating CdTe and HgTe layers of 100−200 Å thickness.
2. In MBE, MCT film growth is carried out at the lowest temperatures (180°C in MBE, compared with 450°C for LPE and 300−400°C for metal organic vapor phase epitaxy). The reduction of growth temperature precludes impurity diffusion from the substrate, thus reducing background doping in the epilayer.
3. Unlike in LPE, no aggressive medium is present in MBE. The absence of an aggressive medium combined with low temperature and analytical facilities for surface control make the use of alternative substrates for growth of epitaxial MCT films possible. Alternative substrates (CdTe or CdZnTe epilayers grown on Al_2O_3, GaAs, or Si substrates) show a definite advantage over bulk CdZnTe substrates in terms of larger possible size, attainability, lower price, and improved matching of thermal expansion coefficient with the read out systems.
4. The main advantage of MBE when using alternative substrates is in the unlimited possibilities of growing different compounds in a single growth system. The advantage of growing multilayer structures in one device is determined by the fact that in MBE no contamination of interfaces occurs. Another advantage of MBE over LPE is that one can control the composition at the interfaces; this makes possible the creation of heterojunctions exhibiting the highest quality.
5. Increased productivity installations for growing MCT and reducing the cost of heterostructures can only be achieved with a high reproducibility of the process. The technologies which are controlled by facilities of built-in analytical processes of growth and preparation of substrates have the advantage, and in this respect, MBE has no competitors.

The implementation of the advantages of MBE, however, require overcoming extremely complex scientific and technological problems, which probably explains why MBE has not become the leading technique in MCT fabrication. High composition uniformity is needed over large areas of the substrate, with a high precision of composition specification and maintenance (<0.005). These are contradictory requirements. Typically, to achieve high uniformity in size the method of MBE substrate rotation is used. However, the rotation of the substrate eliminates continuous use of analytical methods for controlling the composition of the growing layer of MCT, so it is necessary to be guided only by the temperature of the molecular sources. Maintaining the composition method based on temperature control of the molecular sources is not sufficiently precise and reliable, due to the change over time in the amount of evaporated material sources which make it impossible to change the

composition of a controlled thickness heteroepitaxial structure. In connection with this, we developed a MBE chamber design that ensures content uniformity on large area substrates without rotation, which allows continuous monitoring of the analytical methods of the growing process. Ellipsometry is the most suitable method for measuring MCT films composition. The successful application of in situ ellipsometry can uniquely specify the composition of the growing film MCT and can receive structures with a given profile of compositional distribution in thickness.

12.2 Defects Caused by the Use of Substrates From Nonisovalent Compounds

There are two objective factors leading to intensive defect formation in MBE grown A^2B^6 films. The first is due to the low growth temperature for compounds containing mercury. The second is due to the use of substrates from nonisovalent compounds, because substrates of the required size and quality made from the deposited materials have several disadvantages. It is known that intermediate compounds of the $A^3{}_2B^6{}_3$ type are formed at the A^2B^6–A^3B^5 interface [1]. These compounds may influence the growth mechanism and defect formation. In the research on epitaxy, however, one usually studies the influence of the lattice mismatch on the structure of fabricated films. The dependence of the structure of the grown heterosystems on technological growth conditions is also studied (see e.g., Ref. [2]). At the same time, little attention is paid to questions related to the influence of the mutual chemical interaction of the film and substrate components on the film growth and defect formation mechanisms.

We have studied these processes at the initial stage of MBE growth of A^2B^6 compounds on GaAs substrates taking the heteropair ZnSe-GaAs as an example. The ZnSe-GaAs system may be regarded as a model, as ZnSe and GaAs have nearly the same lattice parameters, the tendency to form chemical compounds film components, and the substrate is stronger than that of other systems, such as CdTe-GaAs. The stereochemistry of the surface compounds created from A^2B^6 and A^3B^5 compounds can be successfully studied when the number of valence electrons participating in the formation of surface compounds is taken into account. An excess of valence electrons can lead to a distortion in the tetrahedral configuration of the compounds at the interface (e.g., to an atom i.e., forming two or three, rather than four bonds), and as a result to differing orientations of the film and substrate.

Selenium interacts with GaAs, substitutes arsenic in the GaAs lattice, and forms a chemical bond with gallium [3]. In a lattice with a tetrahedral bond configuration, which is the case for GaAs, there should be four valence electrons per atom. An A^3 atom gives three valence electrons, and a B^6 atom six. As a result, for an A^3B^6 compound there is one extra electron. This is the reason why for A^3B^6 compounds, the tetrahedral lattice turns out to be unstable. Nevertheless, the formation of such a lattice for A^3B^6 compounds is still possible if one third of all the sites in the metal sublattice are vacant. The chemical formula for a compound corresponding to this type of lattice is $A_2{}^3B_3{}^6$. Indeed, in an $A_2{}^3B_3{}^6$ compound there will be $(3 \times 2 + 6 \times 3)/6 = 4$ electrons per site, with vacant sites included.

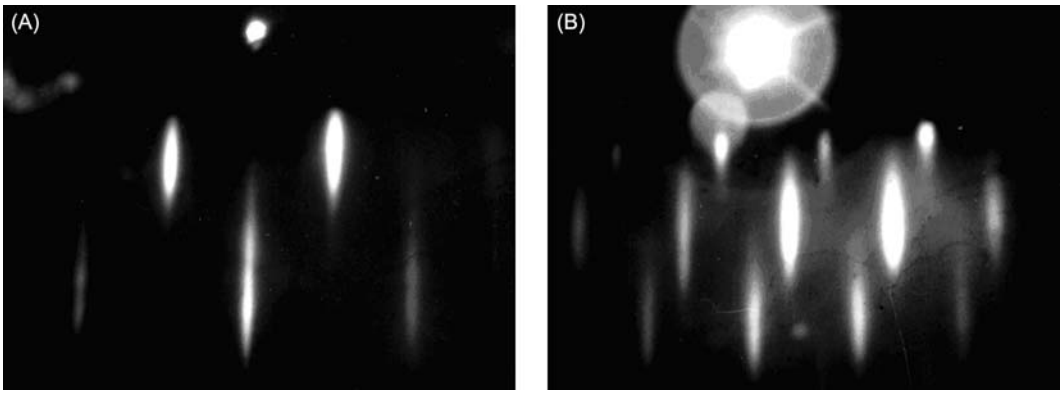

FIGURE 12.1 The diffraction pattern from the surface of GaAs(112)B after preparation with a high content of Se. (A) Azimuth ⟨111⟩, and (B) Azimuth ⟨110⟩.

It should be pointed out that in a crystal lattice with defects, the bonds of group six atoms are not equivalent. There are bonds to the metal atoms and saturated bonds oriented toward the vacant sites. Let us consider the surface of such a crystal formed by a group of six atoms whose saturated bonds have an outward orientation. This surface will have minimal excess energy and will be the most stable, because there are no broken unsaturated bonds on it. Obviously, the (111)B surface corresponds to this configuration of bonds. Therefore, one should expect that crystals of $A_2^3B_3^6$ compounds with a tetrahedral configuration of bonds will favor being faced by the (111)B surface. The formation of a surface with saturated bonds is possible not only for a compact $A_2^3B_3^6$ compound. If a (111)B GaAs substrate is treated with the vapor of a group six element, chalcogen atoms will substitute the arsenic atoms in the surface layer, and also form a surface with saturated bonds.

The epitaxy of A^2B^6 compound films on such surfaces will pose some problems connected with the saturated character of the surface bonds. A possible solution to this situation is the formation of a halogen atom with a six bond octahedral configuration. A hexavalent state is typical for chalcogen. In this case, three bonds of halogen atom direct to the three gallium atoms of substrate, and three bonds direct to the atoms of the second group element of the deposited film. Note that the configuration corresponds to (111)A. It follows that the excess valence electrons on the (111)B GaAs, selenium treated, can lead to a change of polarity (111) on the B(111) to A(111), and the formation of twins during film deposition A^2B^6 compounds.

Thus, the crystal−chemical model heterojunction A^2B^6/GaAs, based on an analysis of the average number of valence electrons per formula unit, predicts that the formation of the lattice with tetrahedral coordination bonds of Ga−Se leads to disruption of the balance of the valence electrons in the heterojunction. An excess of valence electrons on the heterojunction leads to faceting, twinning, and violation of the stoichiometry of the growing structure.

Experiments have shown [4] that steps on the GaAs(112)B surface are formed at sufficiently intensive treatment (temperature and pressure of selenium vapor, see Fig. 12.1); Se peaks in XPS spectra are observed from a surface other than Ga and As peaks.

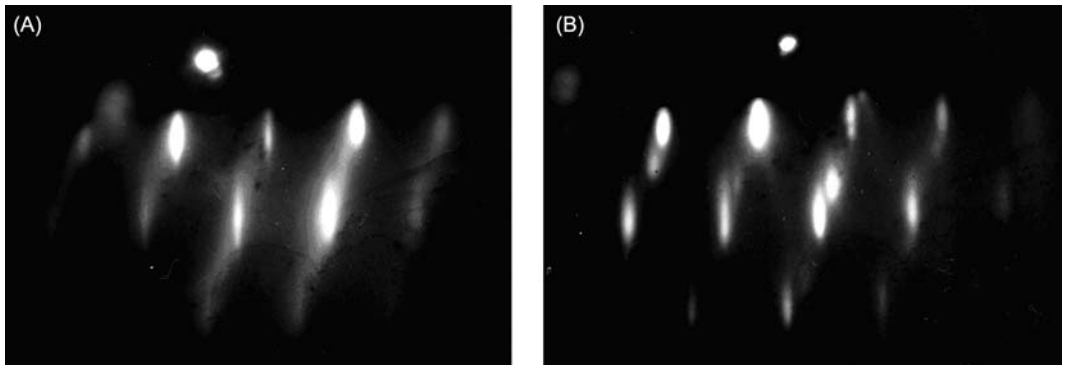

FIGURE 12.2 The diffraction patterns of growth in the initial moment of ZnSe on GaAs(112)B azimuth ⟨110⟩. (A) The growth at 30 s, (B) Growth at 90 s.

This type of pattern is characteristic of the diffraction system of equidistant steps on the surface of the sample along the direction of incidence [4]. It is evident that the splitting reflex multiple of the distance between the reflexes is in the ratio of 1−3. From this, it follows that the ratio between the step width and the identity parameter for (112)GaAs is 3.

Long-term exposure to Se vapor at temperatures exceeding 400°C leads to facets (111). Twinning is observed when A^2B^6 film is grown on such surface [5] (see Fig. 12.2).

The experimentally observed behavior of the surface treated with the molecular flow of selenium, is consistent with the findings of stereochemistry.

12.3 Processes in the Adsorption Layer at MBE $Cd_xHg_{1-x}Te$ and CdTe

Thermodynamic analysis of elemental Te and HgTe crystallization during MBE growth was carried out. The supersaturation was expressed through the Gibbs free energy of the Te and HgTe crystallization [6]:

$$\Delta G_{\mathrm{Te}} = -RT \ln\left[P_{\mathrm{Te}_2}^{1/2}/P_{\mathrm{Te}_2}^{01/2}\right]$$

$$\Delta G_{\mathrm{HgTe}} = -RT \ln\left[\left(P_{\mathrm{Te}_2}^{1/2} \times P_{\mathrm{Hg}}\right)/K_{\mathrm{HgTe}}\right]$$

where ΔG is the Gibbs free energy of the crystallization process, $P_{\mathrm{Te}_2}^0$ is the pressure vapor of tellurium over pure tellurium, K_{HgTe} is the HgTe dissociation constant [7], P_{Hg} is the pressure of Hg at the growth, and P_{Te_2} is the equivalent beam pressure of Te at the growth.

The dependence of ΔG on temperature is shown in Fig. 12.3 [8]. P_{Te_2} is the pressure which is needed for a 1 μm/h growth rate of the HgTe film, $P_{\mathrm{Hg}} = 10^{-3}$ Pa, *solid line*: ΔG_{HgTe} (crystallization of HgTe is possible at $T < T_2$); *dotted line*: ΔG_{Te} (crystallization of Te is possible at $T < T_1$).

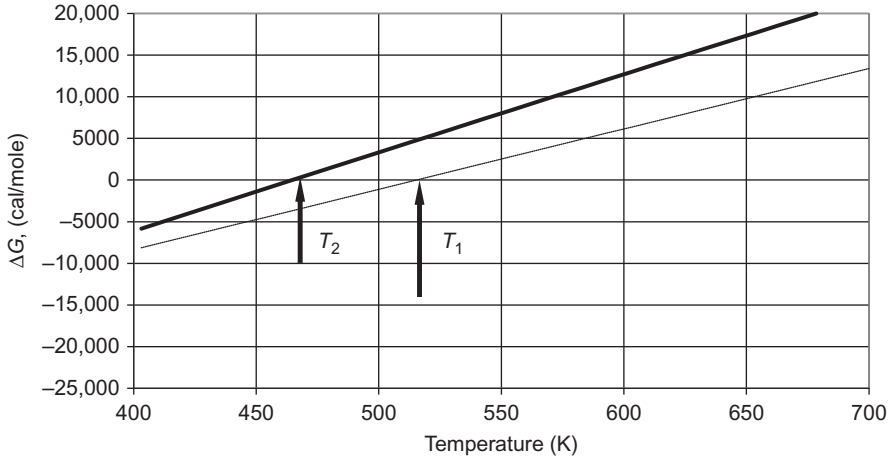

FIGURE 12.3 Calculated dependences of supersaturation on temperature: *solid line*: ΔG_{HgTe} (crystallization of HgTe at $T < T_2$); *dotted line*: ΔG_{Te} (crystallization of Te at $T < T_1$).

At $T_1 > T > T_2$, the single stable solid phase is elemental tellurium. Under these conditions the polycrystalline growth of Te is experimentally observed by RHEED. At $T < T_2$, the stable solid phases are Te and HgTe. The crystallization of these phases will be determined by kinetic circumstances.

A sufficient quantity of mercury on the surface facilitates the formation phase of mercury telluride. When the crystallization of HgTe is complicated (e.g., if mercury adsorption is difficult) the probability of elemental Te crystallization increases.

There are molecules of Te_2 in the molecular beam incident on the growing surface. The dissociation energy of the Te_2 molecule is 54.2 kcal. The diatomic molecule must dissociate into atoms before tellurium can be arranged in a crystal lattice.

As follows from the calculations, the dissociation energy of the Te_2 molecule on a singular surface and near the step decreases to 30 and 10 kcal, respectively. It is clear that in MCT MBE (low growth temperature) a good way of decreasing the Te_2 dissociation energy is to use the vicinal planes of substrates.

12.4 MBE System for Growing Narrow-Gap Solid Solutions Containing Mercury

When designing and building MBE installations for growing narrow-gap solid solutions of mercury, the following requirements were taken into account [9,10]:

1. According to the research into heteroepitaxy $A^{II}B^{VI}$ compounds on GaAs (Section 12.2), a necessary condition for reducing defects in heterojunctions is the absence of vapors of elements of the sixth group at the thermal cleaning of the GaAs substrate from the oxide. Satisfaction of this condition requires the introduction of a special technological installation chamber in which there is no sputtering of elements of the sixth group.

2. Due to the high pressure of mercury vapor, the vacuum system should provide an appropriate means of pumping. The use of a MCT technological module for growing buffer layers is impractical.
3. An automated control system (ACS) for technological processes should ensure the maintenance of precise conditions in the MCT process of growth.
4. The requirement for high composition uniformity layers in the area, together with the requirement for high precision of composition, necessitates the creation of a special tooling chamber for growing MCT, and the introduction of ellipsometric control growth in situ.

Ellipsometric control of the composition is based on the dependence of the MCT optical constants on X_{CdTe}. Thereby, at the angle of incidence $\varphi = 70$ degrees parameter Ψ varies from 4 degrees for CdTe to 15 degrees for HgTe, providing a composition sensitivity of $\delta X_{CdTe} \sim 0.001$.

To get the calibration curve $\Psi(X_{CdTe})$ accurate measurements of MCT films of high structural perfection were obtained by MBE and vapor phase epitaxy [11]. Quadratic approximation of these results (see Fig. 12.4) gives $\Psi(X_{CdTe}) = 14.90 - 13.14X_{CdTe} + 2.36X_{CdTe}^2$. The calibration curve can be recalculated in relation to the measurement conditions in the chamber (angle of incidence and temperature), and allows determination of the composition with an accuracy of $\delta X_{CdTe} = \pm 0.01$, and its relative change during film growth; is no worse than 0.001.

MCT heterostructures were grown on an MBE installation "Ob-M" equipped for operation with mercury [12]. The schematic layout of the system is shown in Fig. 12.5 It includes load-lock and unload-lock chambers. The loading is done in a laminar box. In

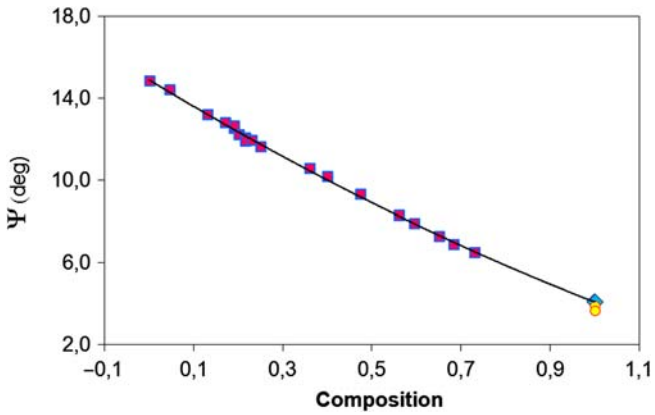

FIGURE 12.4 Calibration curve $\Psi(X_{CdTe})$ for composition determination. *Angle of light incidence is equal to 70°. Symbols are experimental data corresponding to the samples obtained by vapor phase epitaxy (squares), MBE (circles) and cleavage (rhomb);* the *solid curve* is an approximation of experiment by quadratic dependence $\Psi(X_{CdTe}) = 14.90 - 13.14X_{CdTe} + 2.36X_{CdTe}^2$.

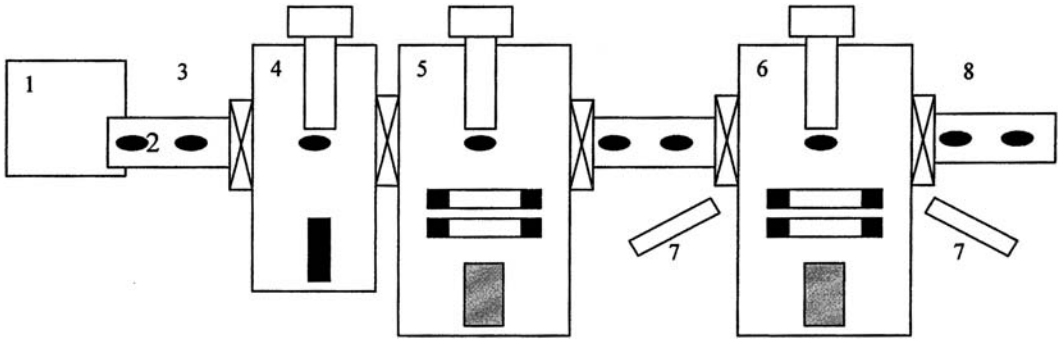

FIGURE 12.5 The scheme of MBE equipment for growing HS MCT. (1) Laminar box; (2) substrate; (3) load chamber; (4) chamber of preepitaxial treatment of substrates; (5) chamber of buffer layers growing; (6) chamber of MCT layers growing; (7) automatic ellipsometer; (8) unload chamber.

this MBE system, three technological chambers are used, with different compositions of the residual gases.

The preepitaxial substrate preparation chamber has an As molecular source. Only thermal treatment of the substrates at a required temperature in the arsenic vapor is performed there. The process is controlled with the help of RHEED.

The chamber for growing buffer layers composed of chalcogenides of group two elements contains vapor of tellurium at a level of 10^{-6} Pa and is, therefore, as has been shown, not suitable for carrying out the procedures of preepitaxial substrate preparation. The chamber is equipped with RHEED and ellipsometer for buffer layer thickness measurements. The chamber for growing narrow-gap solid solutions containing mercury is equipped with a special system of molecular sources providing a sufficiently uniform distribution of solid solution composition without substrate rotation. These sources provide a high uniformity of molecular flows over a large area at a minimum consumption of evaporated materials. Calculations show that the deviation of the composition (x_{CdTe}) should not exceed the value 0.0002 cm^{-1} at the exact alignment. The high uniformity of flow eliminates substrate rotation and implements continuous monitoring of the growth process.

The vapor pressure in the chamber is of the order of 10^{-4} Pa and, therefore, the chamber cannot be used for procedures of preepitaxial substrate surface preparation and buffer layer growth. The control of growth processes was carried out by in situ ellipsometry. An automatic ellipsometer was used for measurements of composition.

The MBE technology installation process is controlled by an automated system. The automated process control system equipment allows you to adjust the temperature of the molecular source and the substrate, and also to control ellipsometry film composition, and manage the growth process. A distinctive feature of the control system is the use of a built-in automated ellipsometer to determine the parameters of the film, with the introduction of feedback on the temperature of molecular beam sources, which allows you to fully automate the process of film growth.

A single-wavelength high-speed ellipsometer (LEF-755) has been developed which can provide control of the MBE MCT processes with its use [13]. No moving parts, as well as an absence of signal modulation during measuring provide a high-speed, which is limited only by digitization. In this device, a single measurement time is 200 ms, with a measurement accuracy $\delta\Psi = \delta\Delta = 0.01$ degrees.

12.5 Growing Heteroepitaxial MCT Structures on a GaAs Substrate

As shown in Section 12.2, surface GaAs(112)B restructuring is possible with the formation of facets (011), (111), and (113) at heteroepitaxy $A^{II}B^{VI}$ compounds on GaAs. ZnTe-CdTe buffer layers are grown on the substrate GaAs to match the crystal lattices of GaAs and MCT. Introduction of a layer of zinc telluride uniquely prevents the change of orientation that almost inevitably occurs during the deposition of cadmium telluride film on GaAs.

Technology developed in ISP SB RAS of MBE MCT used the GaAs substrate (310) [9,10,13]. The surface (310) is not widespread in MBE, and therefore the literature contains no information about its properties. Plane (310) belongs to the ⟨001⟩ zone formed planes (100) and (110). The surface (310) can be obtained by rotating the (100) plane to 19.11 degrees to the plane (110) relative to the [001] axis. It is believed that a system of equidistant steps is formed on the surface at these corners. For the plane (310) azimuth [001] correspond to the direction along the steps, and the azimuth $[\bar{1}30]$ corresponds to the direction across the steps.

In his handbook, Nichols [11] presented an elementary cell of the (310) surface of crystals with a diamond structure. This cell is a parallelogram with an angle forming 122.31 degrees. The handbook provides binding of the cell to two perpendicular directions, $[\bar{1}35]$ and $[\bar{1}3\bar{2}]$. Using the equation of vector geometry it is not difficult to see that the sides of the parallelogram are parallel to [001] and $[\bar{1}3\bar{2}]$, and its small diagonal is parallel to the direction $[0\bar{1}3]$ (see Fig. 12.6).

It was found that, during thermal removal of passivating oxide with GaAs(310) substrate, the most notable changes are observed in the azimuths [001] and $[\bar{1}3\bar{2}]$. As desorption of residual contaminants from the surface of the annealed substrate occurs, diffraction reflexes

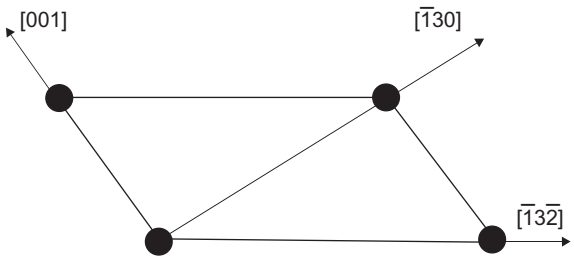

FIGURE 12.6 Elementary cell of the (310) surface of the crystals with diamond structure.

are narrower and stretched. The azimuth $[\bar{1}3\bar{2}]$ fractional reflexes appear, dividing the distance between the main reflexes in half. The azimuth [001] reflexes split, and the diffraction pattern takes the characteristic form of a stepped surface (see Fig. 12.7).

Auger analysis revealed that the thus reconstructed surface comprises O and C in amounts below Auger spectrometer detectivity. This morphological reconstruction surface was chosen by us as a reference point, indicating the receipt of an atomically clean surface of GaAs(310).

Preepitaxial processing of samples was carried out in two ways. The first method was to heat "epi-ready" substrate under a vacuum to remove the passivating oxide, and obtain the appearance of the superstructure (1×2). The second way is to remove the passivating oxide in a hydrochloric acid solution in isopropyl alcohol [14], followed by heating in vacuo until the superstructure appears (1×2). The second method rather than the first allowed us to lower the preepitaxial annealing temperature to 70°C. For a reference point for preepitaxial annealing, temperatures were selected for removal of passivating oxide with "epi-ready" substrate, which was considered equal to 580−600°C, and the temperature of GaAs destruction which is assumed to be 630−650°C. Relative changes in preepitaxial annealing temperature were determined by a thermocouple of the substrate manipulator.

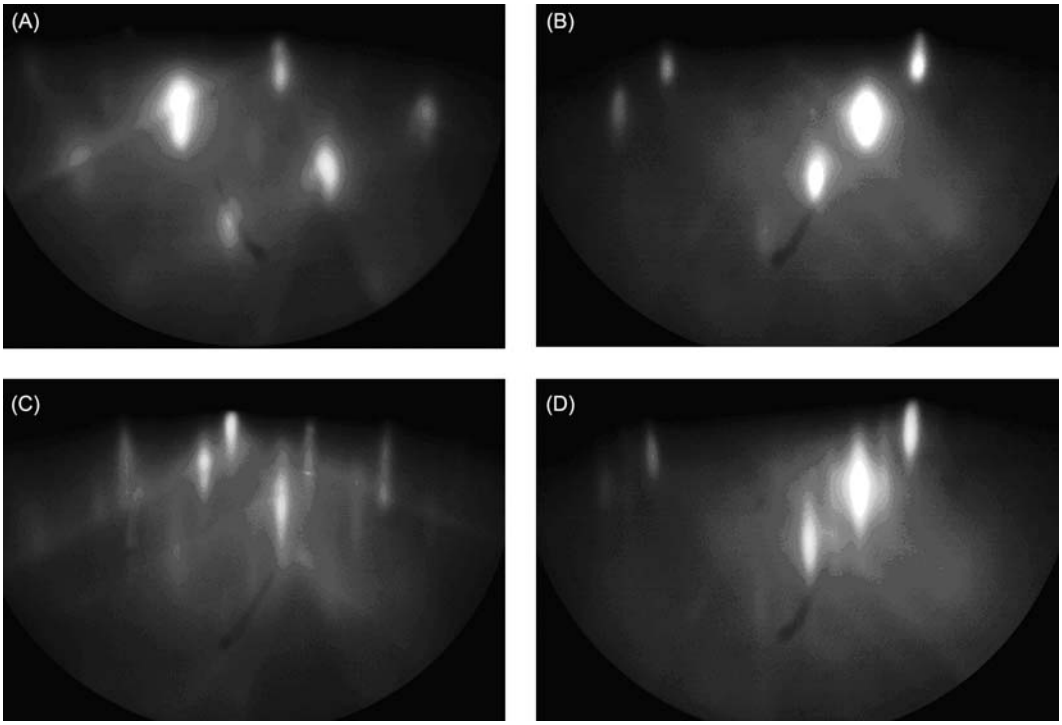

FIGURE 12.7 The diffraction pattern from the surface of GaAs(310) in the azimuth [001] and $[\bar{1}3\bar{2}]$. (A and B) Before annealing; (C and D) after annealing.

Since further considerations of the stoichiometry of the GaAs surface after annealing plays an important role, preepitaxial annealing regimes were tested on the substrate GaAs(100). Annealing at 600°C, and a background As pressure in the chamber of $3.2 \cdot 10^{-4}$ Pa leads to the appearance of an arsenic stabilized superstructure (2×4), which when cooled to 50°C passed to the superstructure (2×3). Therefore, it can be assumed that having the annealing temperature at 500−520°C and a background As pressure in the chamber of $5.6 \cdot 10^{-4}$ Pa should not introduce elemental Ga on the substrate surface GaAs(310).

12.5.1 Zinc Telluride Epitaxy

The pressure ratio of evaporated components has a decisive influence on the morphology of the growing film in MBEMBE of binary semiconductors. The optimum ratio of vapor pressures of groups II and VI components are unknown for ZnTe(310) and CdTe(310) films. Studies have established the following patterns of morphological transformations during zinc telluride and cadmium telluride epitaxy.

If, during growth, Te_2 vapor pressure is greater than the pressure of Zn or Cd vapor, by increasing the film thickness surface roughening occurs. In the diffraction pattern, this leads to a reflex constriction point and lower intensity (see Fig. 12.8B). If, during the growth, the vapor pressure of Zn and Cd is more than the Te_2 vapor pressure, an atomically smooth surface will be formed during epitaxy. The diffraction pattern from such a surface is characterized by narrow reflexes, sharp Kikuchi lines, and low diffusion background (see Fig. 12.8A).

12.5.2 Epitaxial Growth of Cadmium Telluride

A converging spiral-like curve in the $\Psi-\Delta$ plane is observed with the growth of cadmium telluride films on a GaAs substrate. The start point corresponds to GaAs, and the end point corresponds to bulk cadmium telluride. There is good agreement between the theoretical curve

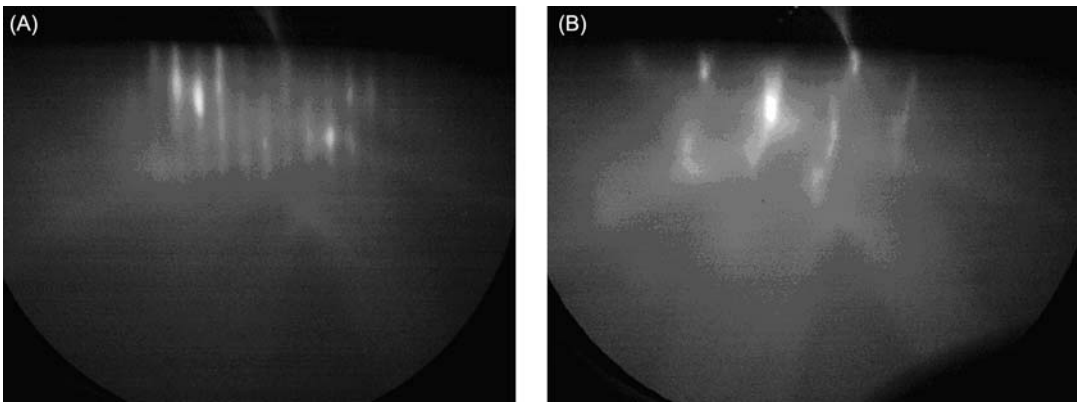

FIGURE 12.8 Diffraction patterns in azimuth [001] from the surface of CdTe(310) 5 μm thickness film. (A) Film grown under conditions $P_{Cd} > P_{Te}$, $T_S = 280$°C. (B) Restructuring of the surface shown in Fig. 5.3a at Te adsorption, $P_{Te} = 1 \cdot 10^{-5}$ Pa, $T_S = 210$°C.

and the experimentally measured Ψ, Δ. This fact allows the determination of the epitaxial film growth rate. However, in the case of nonoptimal growth conditions, a deviation of the measured ellipsometric parameters from the theoretical curve takes place [15].

The same as for zinc telluride, there is an optimal ratio of cadmium and tellurium flows, providing epitaxial cadmium telluride growth with the best structural perfection. For these growth conditions, the surface state must not be changed, i.e., no surface morphology should be developed. As in the previous case (zinc telluride growth), surface relief is equivalent to a layer with different optical constants. The angle delta (Δ) is the most sensitive of ellipsometric parameters to relief. Fig. 12.9 shows the evolution of ellipsometric parameter Δ for three cases of CdTe epitaxial growth. The conditions of surface preparation were identical in all cases, as well as the ZnTe buffer layer growth conditions. In these experiments, the CdTe growth rate was 2.1 μm/h, and the growth temperature $T = 290^{\circ}$C. In the case of the optimal flow ratio $J_{Cd}/J_{Te_2} = 3.5$, changes in the ellipsometric parameters Ψ and Δ do not occur. When CdTe film is growing with a large excess $J_{Cd}/J_{Te_2} = 27$, a weak monotonic decrease of ellipsometric parameter Δ occurs. While growing CdTe film in conditions close to tellurium enrichment, $J_{Cd}/J_{Te_2} = 1$is accompanied by a sharp decrease of ellipsometric angle Δ by a value of ≈ 30 degrees at an early growth stage. Using this method, optimal process conditions for growing CdTe films were determined.

Epitaxial layers of CdTe, grown on ZnSe/GaAs(013) substrates with optimal technological parameters ($J_{Cd}/J_{Te_2} = 5 - 7$, $T_{sub} = 280{-}290^{\circ}$C, growth rate ≈ 2 μm/h) have the best structural perfection (half-width of the X-ray rocking curve ≈ 2 angular minutes for 6 μm film thickness). The surface topography of such films, as shown by AFM studies, did not exceed 4 nm.

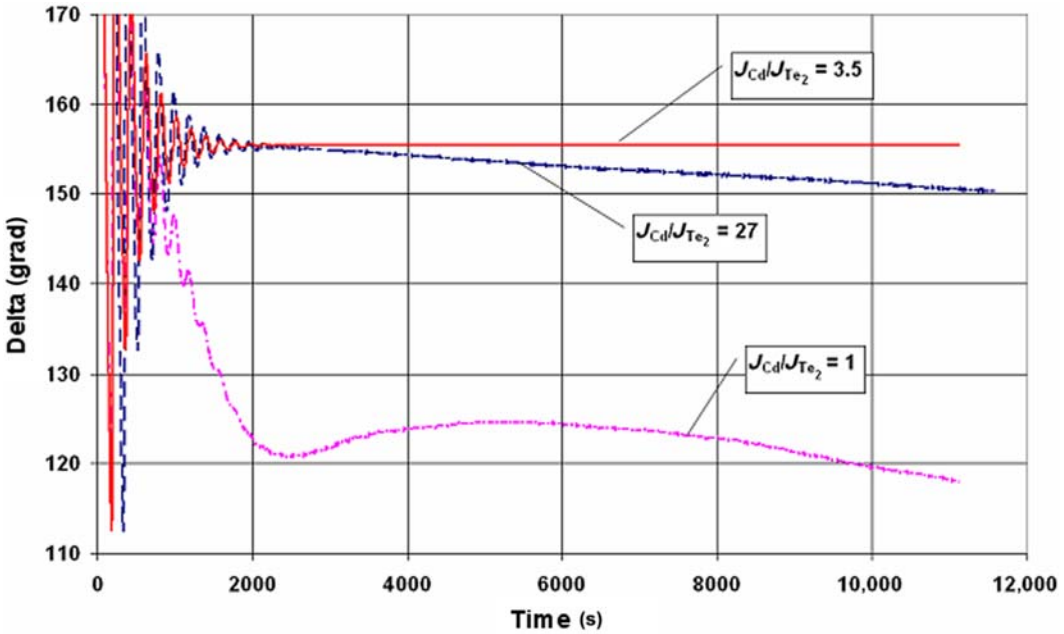

FIGURE 12.9 Changing the ellipsometric parameters during CdTe film growth.

12.5.3 MCT Growth

Growing MCT epitaxial layers were produced from separate sources of Cd, Te, and Hg. The special design of the sources, and their location in the growth chamber is described in Section 12.2. Monitoring the work of molecular sources, of the mercury flow sensor, of the substrate temperature, and of an automatic ellipsometer LEF-755, as well as process control, was carried out with the help of ACS [16].

Mode component flows in growing MCT differ substantially from the molecular flows. Molecular fluxes are considered when the atoms or molecules are not experiencing collisions when moving from the source to the growing surface. In a typical substrate, a temperature of 165−200°C is desired, and mercury vapor pressure above the growth surface should be no less than 10^{-3} Pa. Under these pressures the mercury flow influences on the value of tellurium flux coming onto the substrate. Mercury flow change also affects the amount of cadmium flow. Deposition of tellurium film on a cold substrate in the presence of mercury, and in the absence thereof, showed a significant change in the growth rate of the film of tellurium. Growth rates are reduced by 2−4 times with increasing mercury vapor pressure. Therefore, cadmium and tellurium flows arriving at the substrate surface substantially change when the mercury flow changes.

As noted in Section 12.3, tellurium falls on the surface in the form of diatomic molecules. Tellurium vapor pressure at the substrate temperature is small. If the diatomic tellurium does not react with mercury and cadmium, it cannot evaporate, and remains on the surface to form a tellurium solid phase. Thermodynamic analysis shows that at temperatures less than 190°C two stable phases may exist at the same time, crystalline phase tellurium and MCT [9]. In this case, the preferential formation of one or the other phase will be determined exclusively by the kinetics of formation of the corresponding phase.

Fig. 12.10 schematically shows the main possible processes occurring on the surface with tellurium. Tellurium molecules on the surface are involved in two processes: the dissociation

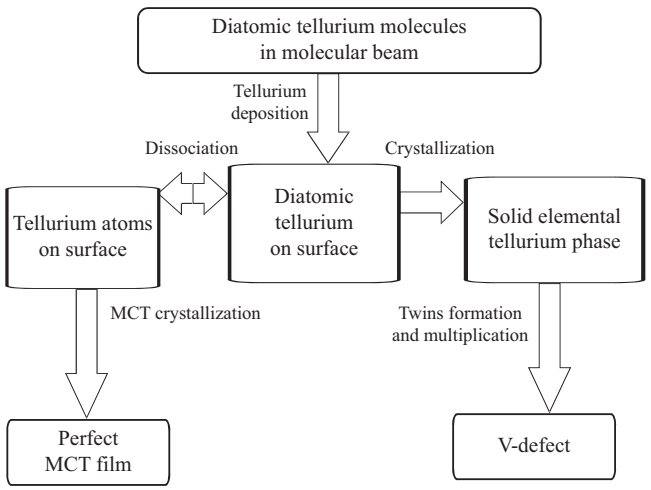

FIGURE 12.10 Processes involving tellurium occurring on the MCT surface.

of tellurium molecules and crystallization of perfect film MCT, and tellurium crystallization as a separate phase when the dissociation process does not have time to take place. In the latter case, the formation of a tellurium phase on the surface suppresses the crystal growth of MCT, and leads to an avalanche of defects. As a result, under optimum conditions, it is possible to observe irreversible deterioration of the crystal structure and HgCdTe surface relief development.

The MCT growth process is controlled in a "Ob-M" vacuum chamber with the automatic ellipsometer LEF-755 only. As in the case of buffer layers, at the initial stage of MCT growth one can observe the trace of ellipsometric parameters in the form of a convergent spiral (in the $\Psi-\Delta$ plane) due to the existence of a CdTe−HgCdTe interface. The results of these measurements are shown in Fig. 12.11 [17].

These results at the initial stage of growth allow determination of the film growth rate when the thickness and growth time are known. The point of the twisting "snail" allows us to determine the composition of the growing layer from the calibration curve (see Fig. 12.4). In accordance with the thermodynamic concepts discussed in Section 12.3, there is an opportunity to grow MCT films with different composition without substantially changing the technological conditions. Therefore, to reduce the impact of heterojunction and surface recombination of charge carriers (see Section 12.5 for more detail), it is typical to grow the structure represented in Fig. 12.12. On the heterojunction

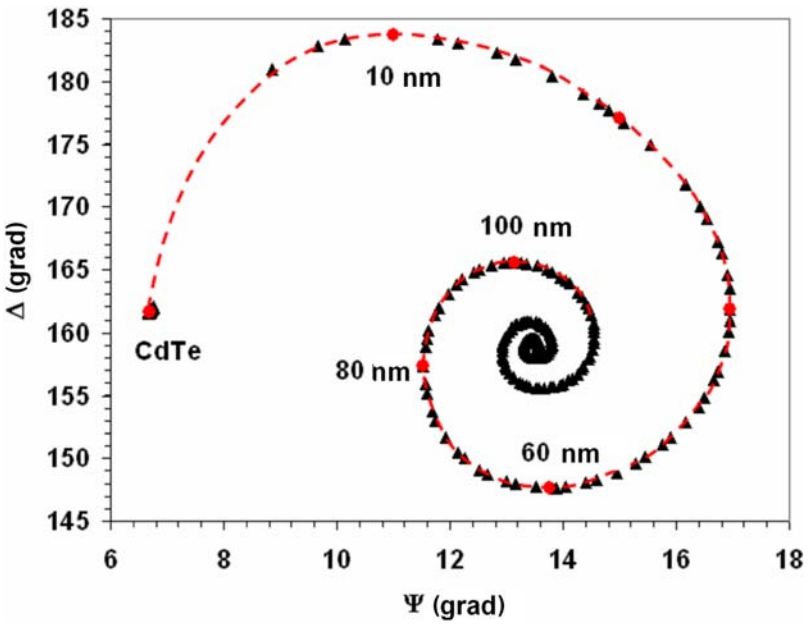

FIGURE 12.11 Variation of the ellipsometric parameters during growth of a MCT film on a CdTe substrate at an initial stage. The *dashed line* shows the calculated curve. Numbers near the circles indicate film thickness in nanometer. *Triangles* are experimental results.

with the buffer layer and near the surface more wide-band layers are grown. The inset in the figure shows the temperature change measured during the growth process by a polarizing pyrometer. It would be seen that during growth the substrate temperature is able to keep within $\pm 1.5^{\circ}C$. Therefore, the composition accuracy during growth will not be worse than $\Delta X_{CdTe} = 0.001$. This fact is also confirmed by the following transmission spectra measurements [13], with step-by-step etching of the surface layer. It can be seen that there is complete agreement between the results of in situ ellipsometric measurements and stratified etching.

Thus, when the film grows in optimal conditions, we can precisely control the composition of the growing film. Ellipsometric in situ monitoring of the growth process allows us to grow potential barriers precisely, as well as potential wells, by growing built layers with different compositions. When growing the MCT nanostructures a high growth rate should be maintained in order to reduce growth time, and thereby reduce the influence of elements of interdiffusion. For precise control of composition and thickness, using the ellipsometric technique during real rates growth of MCT (3−5 μm/h) is necessary to ensure high speed and threshold sensitivity of the measurements [18].

When growing thin nanolayers (barriers or quantum wells) there are two interfaces formed, so the trajectory of the ellipsometric parameters will consist of two spiral curves. The shape of these curves is determined by the composition, and their extension by the layers' thickness. Fig. 12.13 [18] shows the variation in the ellipsometric parameters measured with a sharp decrease of the tellurium flux in a short time (∼1 s.) by the partial overlap of the molecular tellurium source. Experimental results are shown by the symbols.

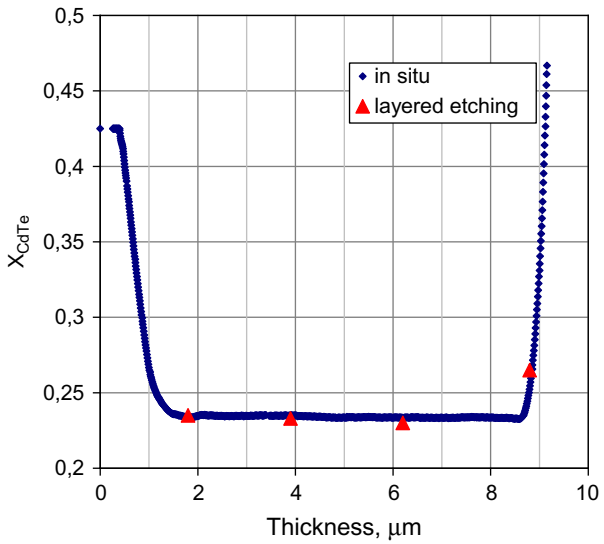

FIGURE 12.12 Composition distribution across thickness of HgCdTe MBE film measured by in situ ellipsometer. Triangles are composition measurements during step-by-step etching the epitaxial film.

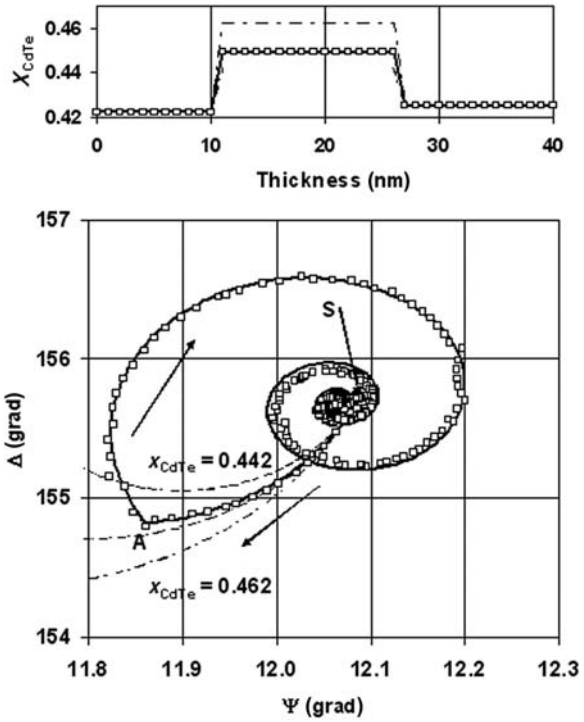

FIGURE 12.13 Ellipsometric parameter variation during growth of potential barrier of composition $X_{CdTe} = 0.449$ on the MCT substrate of $X_{CdTe} = 0.22$. The upper part of the picture: Dependence of the growing films composition on thickness; Lower part: Ellipsometric parameter variation. *Squares* are the experimental measurements, the line is a single-layer model. *Dashed curves* are modeling the potential barriers of composition $X_{CdTe} = 0.442$, 0.452, and 0.462. The *arrows* show the sequence of ellipsometric parameter variation. Point S corresponds to the initial composition. Curve SA corresponds to composition of the barrier layer.

Intervals between measurements are 1 s. The start variation (point S) corresponds to the steady growth of MCT with the composition $X_{CdTe0} = 0.422$. After shutting-off Te flow, there is a rapid change of parameters Ψ and Δ along the line SA. In accordance with the modeling conducted above, the area SA represents part of a spiral curve corresponding to a growing layer with a higher content of CdTe. After Te flow restoration, there is a break at point A of the ellipsometric parameters trajectory, which continue to change by drawing another spiral curve convolving to the starting point S.

The coincidence of the start and the end points of the process means that, after restoration of the Te flow, the composition of the growing MCT film returns to its initial value X_{CdTe0}. The composition profile is shown in the insert, and the calculated curve describing variation of ellipsometric parameters for this profile is represented by a *solid line* in the figure. The good agreement between the theoretical curve with the experimental data which occurs after Te flow restoration (part AS) proves the growth of a uniform layer with constant composition. A slight discrepancy corresponds to a composition change of a few thousandths

mole fraction. The break of the experimental trajectory at point A shows a stepped composition change; the transition layer thickness is no more than 0.5 nm. The thickness of the barrier layer is determined by the length SA, and in this case it is 16.2 ± 0.1 nm.

In Fig. 12.13 *dotted lines* show parts of the curves calculated for barrier layer composition exceeding X_{CdTe0} at 0.02, 0.04, and 0.06 mole fraction. Comparing these curves with the experimental results one can see that the composition of the barrier layer is $X_{CdTe} = X_{CdTe0} + 0.027$, and accuracy is $\delta X_{CdTe} = \pm 0.002$.

It should be noted that the accuracy of determining the thickness and composition of grown nanostructures strongly depends on the absolute value of the layer thickness. From the results we can conclude that, for structures having practical application with a thickness of 10 nm, the ellipsometric technique provides the necessary accuracy of nanolayer thickness and composition, and also allows you to control the quality of the interface.

The above analysis shows the ability for controlled growth of the potential barriers and wells on the basis of solid solutions $Cd_xHg_{1-x}Te$. In the report of the Academy of Sciences of the USSR in 1987 a manuscript was published by our colleagues A.V. Rzhanov, K.K. Svitashev, A.S. Mardezhov, and V.A. Shvets about the possibility of ellipsometric control during the preparation of superlattices based on alternating layers of CdTe and HgTe [19].

The experiments showed [20] that ellipsometric control really enables the necessary accuracy for both the composition and thickness in growing embedded potential barriers and wells (when composition varies at any desired interval, and layer thickness is from a few to hundreds of nanometers), as well as when growing smooth varying band structures with the required variation of the composition gradient. An example of the grown structures with 30 HgTe quantum wells and wide-doped electrodes is shown in Fig 12.14.

Fig. 12.14 on the left side shows the structure of the quantum wells, the diagram on the right side is of the ellipsometric parameter variation during the growth of 30 HgTe QW. One can see that there is a piece-wise smooth curve during growth. The blue color shows the variation of the ellipsometric parameters during growth of wide-doped electrodes, and the red curves show HgTe QW.

12.5.4 The Nature of V-Shaped Defects in HgCdTe Epilayers Grown by MBE

Typical threading defects, which are called voids [20–22] or surface-craters, are commonly observed on the surfaces of HgCdTe epilayers grown by MBE. The cross-sizes of these defects extend to the top surface, so we called them V-shaped defects [23,24]. A typical density of V-shape defects is about 10^3 cm^{-2}. When a V-shaped defect is located within the active area of a photodiode it leads to a deterioration in diode parameters. Because of this, the density of V-shaped defects must be minimized, especially for fabrication of focal plane infrared detector arrays. In spite of the importance of this problem, the mechanism of nucleation and multiplication of defects during MBE have not been well investigated. The important role of elemental Te in the formation of V-shaped defects was shown in Ref. [24]. Several groups [20,25] demonstrated a reduction in defect density to 100–300 cm^{-2} by

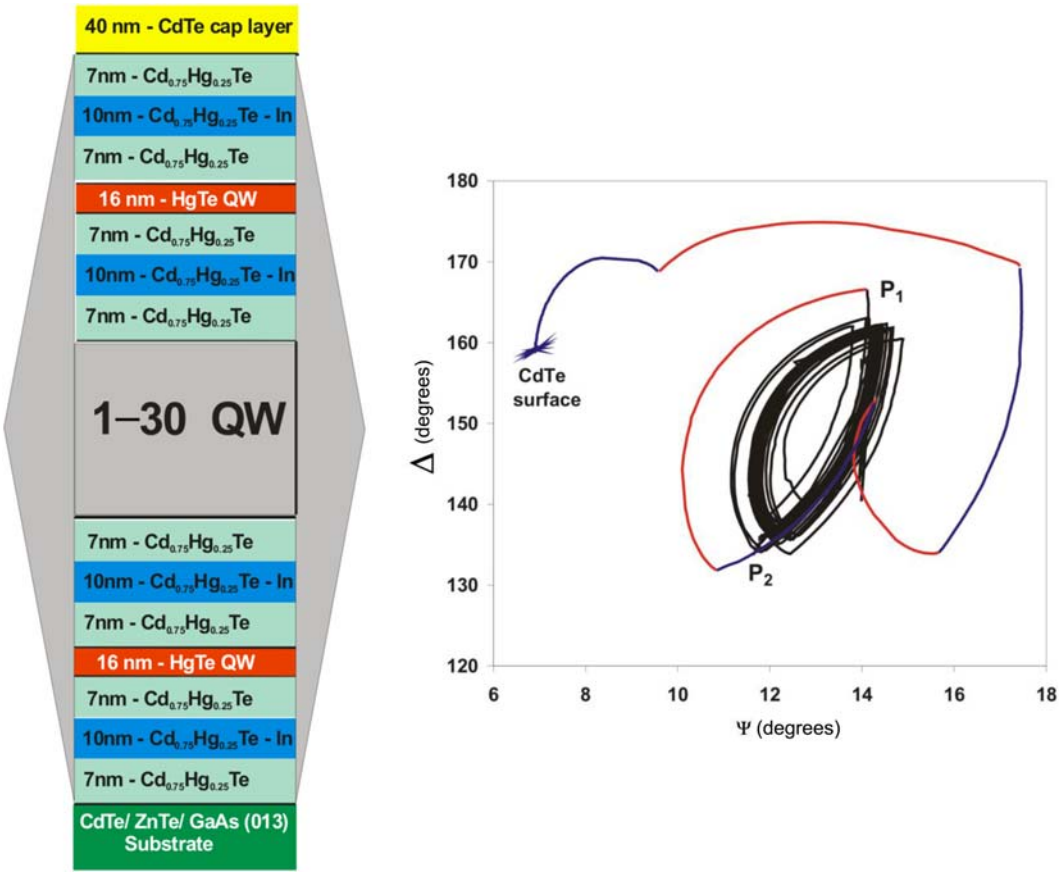

FIGURE 12.14 On the left side is a cross-sectional view of the structure, and on the right side are the ellipsometric parameter variations during the growth of 30 HgTe QW.

optimization of growth conditions and careful preparation of substrates. For reproducibility and improvement of this result, in our opinion, it is necessary to investigate the microstructure and mechanism of V-shaped defect formation in detail.

AFM and TEM investigations show [26] that V-shaped defects are complicated defects composed of twin lamellas, stacking faults, and areas with disordered structure with a high concentration of elemental Te, that can be up to 3% according to electron probe microanalysis [8] (see Fig. 12.15). Close to V-shaped defects, typical surface irregularities are observed.

Fig. 12.15 shows the typical AFM (A) and TEM (B) images of V-shaped defects observed on (301)HgCdTe surface. A comparison and analysis of these images allows us to find the correlation between the peculiarities of micromorphology in the defect area and its microstructure. Fig. 12.16 shows the scheme for the analysis of V-shaped defect images. In this scheme the pyramid formed by {111} planes inclined to the (301) surface (A) and the quadrangle trace of intersection of this pyramid with the (301) surface (B) are represented.

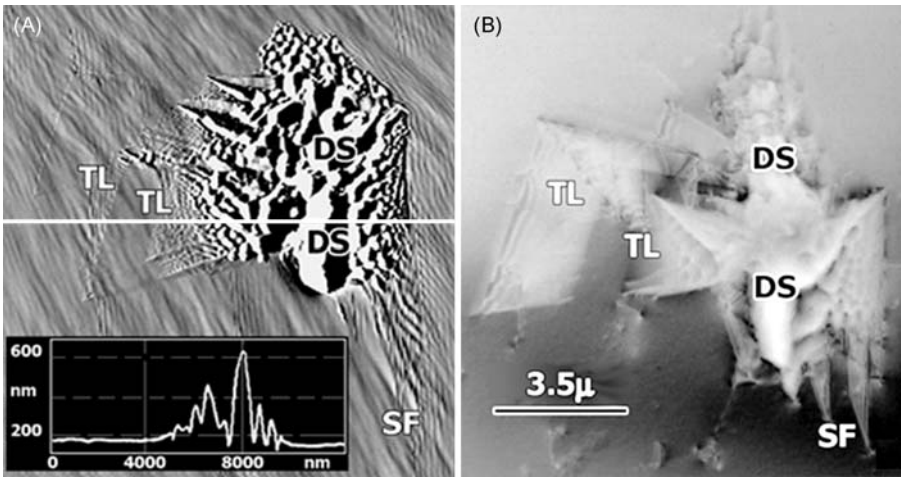

FIGURE 12.15 Typical AFM-image, $12 \times 12\ \mu m^2$ scan (A), and TEM-image (B), of V-shaped defects composed of twin lamellas (TL), stacking faults (SF), and disordered structure areas (DS) on the surface of (301)HgCdTe film. The insert in (A) shows the relief profile along the *white line*.

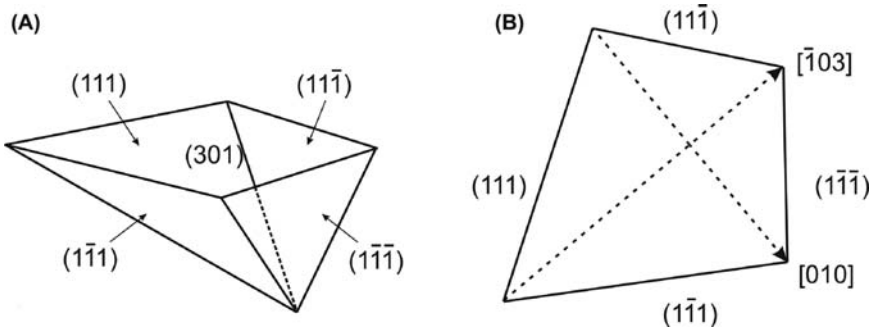

FIGURE 12.16 The pyramid formed by {111} planes inclined to (301) surface (A), and the trace of intersection of this pyramid with (301) surface (B).

In Fig. 12.15 we see the typical elements of V-shaped defects: SFs, TLs, and DS areas. The height profile along the white line in (A) is shown in the inset. The height of the DS-area is over 500 nm. The SFs and TLs grow along {111} planes from the V-shaped defect center. When a V-shaped defect image is compared with the scheme shown in Fig. 12.16, it is evident that the defect is bounded to the right by the $(1\bar{1}\bar{1})$ plane which is inclined at 68.58 degrees to the (301) plane, and to the left by a set of (111) planes which are inclined at 43.09 degrees to the (301) plane. TEM investigation of cross-sections shows that essentially all SFs observed in (301) HgCdTe layers are located in $(1\bar{1}\bar{1})$ planes, growing from the CdTe buffer layer. SFs which lie in the (111) planes are observed only in the area of V-shaped defects. The areas with disordered structure in the center part of the V-shaped defect are the most hazardous to photodiodes.

Thus, the formation mechanism and microstructure of these areas were closely studied. At low defect density (less than 10^3 cm^{-2}) TEM investigation is difficult because of the small size of the e-transparent foil area and low defect density. To follow the consecutive stages of V-shaped defect formation by TEM, it is best to use the growth of HgCdTe layers under nonoptimal conditions: elevated temperatures and reduced Hg−vapor pressure. Under these conditions, continual V-shaped defect nucleation takes place, and defect density may be as great as 10^6 cm^{-2}.

The analysis of this TEM image reveals the consecutive stages of V-shaped defect formation, beginning with the initial ones shown in Fig. 12.17A. The lines (line-shape areas) of disordered structure are seen along the macrostep bends as dark lines with diffraction contrast. The microstructure along these lines was observed with atomic resolution. The HREM image shows the presence of precipitates with the distance between atomic layers precisely the same as in elemental Te (0.59 nm) (see insert in Fig. 12.17B).

Fig. 12.17C shows the presence of misoriented fine HgCdTe grains. Since Te activity during HgCdTe growth by MBE is sufficient for elemental Te formation [9], it would appear reasonable to assume that under nonoptimal conditions elemental Te can be accumulated along the growth front (along the macrosteps in the case of steady state growth) and can initiate the nucleation of misoriented HgCdTe grains and Te precipitates, at a size of 10 nm.

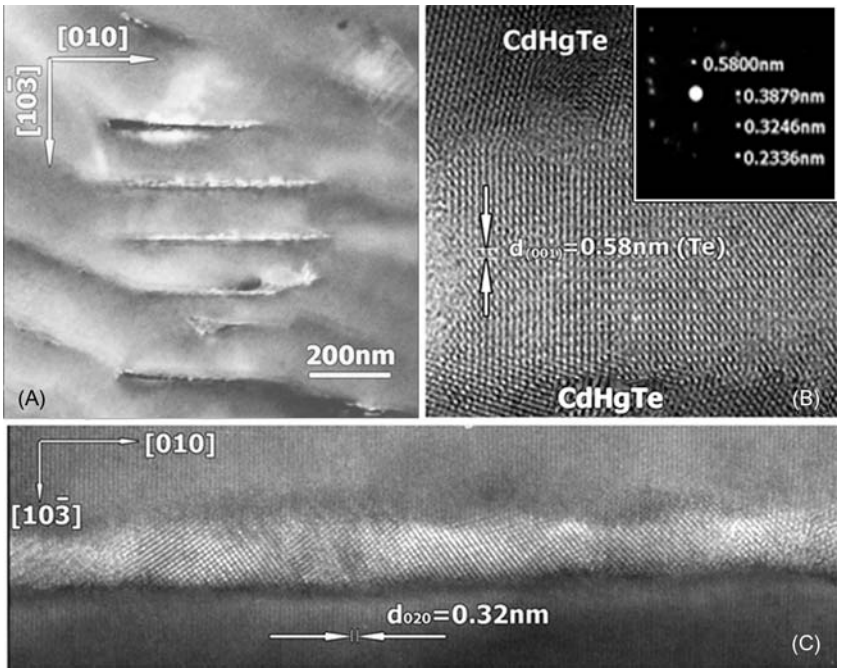

FIGURE 12.17 Initial stage of V-shape defect formation. (A) Bright field TEM-image of disordered structure that is formed along [010]-macrosteps, $g = 040$; (B) HREM-image and corresponding microdiffraction pattern of Te precipitates; (C) HREM-image of misoriented fine HgCdTe grains that are formed along [010]-macrosteps; the orientation of the HgCdTe grains is close to (001). The incident e-beam direction is [301] (A and C) and [110] (B).

In these places the macrosteps bend because its flow is pinned. As a result, short lengths of macrosteps can assume an exact [010] direction, as follows from the TEM data.

HgCdTe grains and Te precipitates can trigger the formation of dislocations, which are also observed along the macrostep bends (Fig. 12.17B). At this stage, the formation of walls with HgCdTe grains, excess Te, and dislocations begins, while HgCdTe layer growth in these walls with disordered structure extends along the growth direction.

Hereafter, we shall use the term " DS-walls" to mean the walls with disordered structure. Stereophotography was used to locate these DS-walls. The DS-wall images shown in Fig. 12.17A have been obtained under imaging conditions close to the [301] zone axis (when the incident e-beam direction is perpendicular to the (301) surface). Under these conditions, the width of the DS-wall image is minimum. When the sample is tilted 18 degrees about the [010] axis to the left (toward the (100) pole), and to the right (toward the (101) pole) the DS-wall image becomes wider and appears to the right and to the left from the [010] direction respectively. This indicates that DS-walls are normal to the (301) growth surface. The DS-walls observed by TEM intersect the (301) growth surface in the [010] direction. From analysis of a stereographic projection for the (301) plane, it follows that DS-walls are located in vertical (103) planes, which are perpendicular to the (301) plane and intersect it along the [010] direction. The formation of DS-walls which extended along the growth direction and contained HgCdTe grains, Te precipitates, and dislocations, and may be considered the initial stage of V-shaped defect formation. In the initial stages of HgCdTe layer growth the situation is complicated by the fact that the optimal growth conditions are not attained yet, whereas the relief perturbations on the substrate surface are present. In the experiments carried out the CdTe buffer layer plays the role of a substrate. Our investigation of CdTe buffer layers by TEM and AFM revealed that surface irregularities with a height of more than 10−20 nm are the result of threading defects.

Thus, the study of the microstructure and micromorphology of V-shaped defects in films $Cd_xHg_{1-x}Te(301)$ in successive stages of their formation by TEM, HRTEM, and AFM allowed elucidation of the mechanism of formation of V-defects in MBE $Cd_xHg_{1-x}Te$ [26]. The formation of the V-shaped defect begins from the capture of excess Te along the growth front at steady state stages of HgCdTe growth, and along the irregularities on the surface of the CdTe buffer layer at the initial stages. The captured Te initiates nucleation of misoriented HgCdTe grains, new Te precipitates, and dislocations in the vertical walls that are formed along the growth front under nonoptimal growth conditions. It was established that the formation of these walls with disordered structure (DS-walls) extended along the growth direction in the initial stage of V-shaped defect formation. Under the effect of strains, the splitting of perfect dislocations into partial ones with SF between them takes place. DS-walls bound the gliding of partial dislocations and lateral SF growth. While growing, the vertical columns packed with SFs and bounded by DS-walls are formed. These columns represent the basic part of the V-shaped defect—DS-area. Due to the continual Te nucleation and twinning, the polycrystalline growth in DS-area can occur. The extended SFs and TLs grow from the DS-areas along {111} planes. With film thickness growth, the size of DS-areas increases as well as the size of extended SFs and TLs. As a result, the lateral size of the V-shaped defect increases with increasing HgCdTe film thickness.

12.6 The Homogeneity of the Composition and Electrical Properties of Heteroepitaxial of MCT on a GaAs Substrate

MCT growth is highly sensitive to the orientation of the substrate surface. It was established experimentally that the orientation of gallium arsenide (103) is optimum for growing MCT. It helps to prevent the formation of twins, twin lamellae with the growth of II−VI compounds. This orientation is less sensitive to changes in the conditions of the growing process, and allows a single process to carry out the growth of MCT films of various compositions.

The composition distribution on the area of the films grown on GaAs substrates with a diameter of 76.2 mm, was measured using the spectra of transmission on a Bruker Fourier spectrometer with local measurements of 0.5 mm^2. We obtained the following composition distribution characteristics: X_{CdTe} mean = 0.20171, standard deviation $\Delta X = 0.000164$, and relative deviation $\Delta X/X = \pm 0.654\%$. This uniformity in the HS diameter of 76.2 mm compared to the best published data obtained by rotating the substrate [27].

Thanks to *in situ* ellipsometric control the MCT layers may have a predetermined composition profile, e.g., the working layer of constant composition and graded-gap layers. Fig. 12.12 illustrates the change in the composition of the thickness of typical HS MBE MCT layers with graded-gap measured by ellipsometer during the growth process. When the composition of the working layer of $X_{CdTe} = 0.22$ at the boundaries of the working layer created variband layers, the CdTe content rises to the surface and to the border with the buffer layer. Graded-gap layers with a high content of CdTe can be used to passivate the surface [28]. The increase in the band gap on the surface of the MCT and heteroboundaries film creates built-in fields, brushing aside nonequilibrium carriers from surfaces which can have high recombination rate. There is reason to believe that in this way you can increase the effective lifetime of nonequilibrium carriers [29]. Fig. 12.18 shows an example of the composition

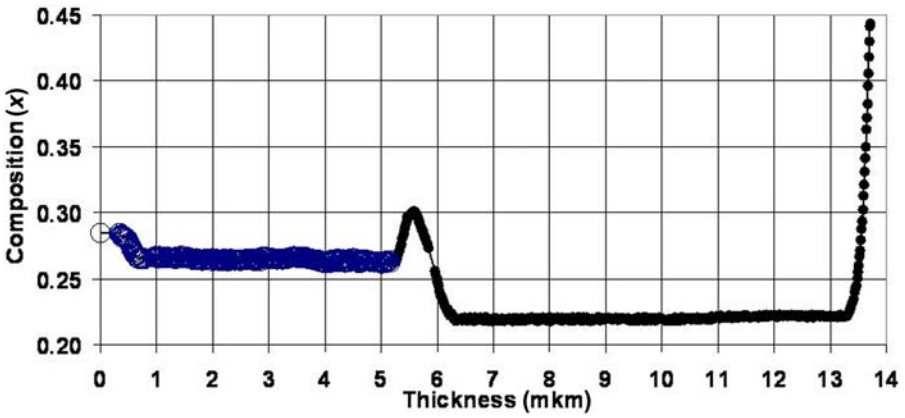

FIGURE 12.18 The results of in situ ellipsometry measurements of the film thickness: a sublayer 5 μm thick, a wide-layer between the working layer and sublayer, and the graded-gap layer on the surface.

distribution in a structure with a sublayer ($X_{CdTe} = 0.27$) with high conductivity, which can be used to decrease the series resistance in large format arrays and diode heterodyne. To prevent recombination of nonequilibrium carriers, the sublayer is separated from the active layer ($X_{CdTe} = 0.22$) by a wide-gap layer ($X_{CdTe} = 0.30$).

As-grown the MCT films are of n-type conductivity. The concentration of carriers in n-type films are in the range of $1 \cdot 10^{14}\,cm^{-3}$ to $1 \cdot 10^{15}\,cm^{-3}$ at mobilities of 50,000−150,000 cm^2/V s. Fig. 12.19 shows the dependence of carrier mobility in n-type material versus layer composition. The experimental values (*dots* on Fig. 12.19) agree well at liquid nitrogen and room temperatures with the theoretical values (*solid lines* on Fig. 12.19) from Ref. [30], calculated under the assumption that the dominant scattering by optical phonons. Mobility for the composition $X_{CdTe} = 0.158$ reaches 710,000 cm^2/V s at a temperature of 77K, and is comparable with the best mobility in the bulk material.

One of the most important parameters of the materials used for the manufacture of photodetectors is the lifetime of photoexcited carriers whose value is largely determined by the presence of recombination centers in the films. Layers of HgCdTe n-type conductivity with graded-gap layers at 77K have a record high minority carrier lifetime for material grown on a GaAs substrate. The temperature dependence of the lifetime of minority carriers in the film with $X_{CdTe} = 0.22$ is shown in Fig. 12.20. After etching, the upper variable-gap layer relaxation time of nonequilibrium carriers at a temperature of 77K is reduced by 4−5 times, indicating the positive effect of graded-gap layers. It should be noted that the carrier concentration in MCT structures with graded-gap layers does not differ from one of the structures without graded-gap layers. Perhaps dislocation does not affect the lifetime as much as it is thought.

n-type films are transferred to p-type conduction at a concentration ranging from $5 \cdot 10^{15}\,cm^{-3}$ to $2 \cdot 10^{16}\,cm^{-3}$ at mobilities of $300 - 600\,cm^2/Vs$ of annealing temperature

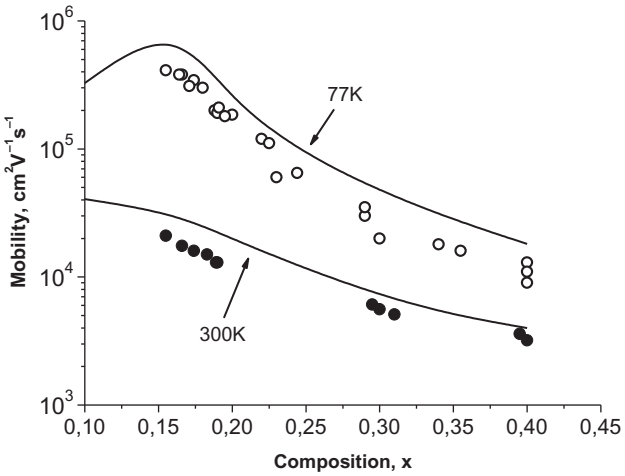

FIGURE 12.19 Mobility dependence on the composition of the MBE MCT films.

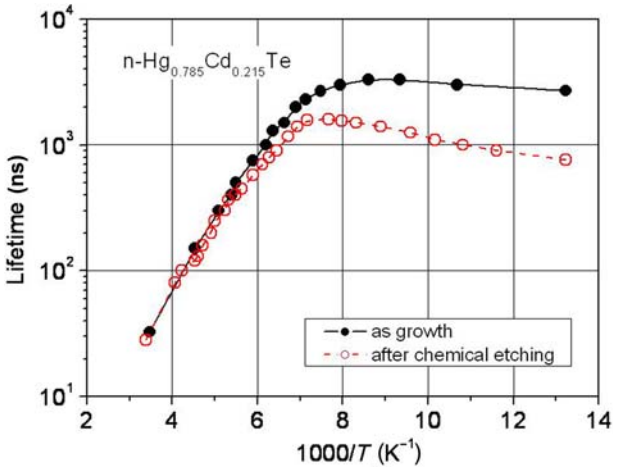

FIGURE 12.20 Temperature dependence of the minority carrier lifetime in HgCdTe, $X_{CdTe} = 0.22$.

230°C, mercury temperature 30°C, and an annealing duration of 20−40 h. Heat treatments used an ampoule filled with gas (hydrogen or helium). Dependence of the results of annealing on the type of gas were not observed. The ampoule was placed in a two-zone furnace. One zone is intended for heating the reservoir with mercury, and the second is used to heat the sample. Changing the conductivity type is reversible, annealing at a temperature of 230°C and mercury temperature above 180°C again gives n-type conductivity. The calculation of the temperature dependence of the concentration of vacancies in the composition range $X_{CdTe} = 0.2-1.0$ [31] makes it possible to determine the optimal parameters of heat treatment in graded-gap and multilayer structure MCT in order to obtain the desired profile of the concentration of vacancies.

The experimental evidence on the effect of annealing conditions on the properties of the films MCT suggests the presence of MCT films using GaAs substrates, in addition to moving acceptor centers with variable concentrations and also donor centers, the concentration of which depends on the growing conditions. The main donor centers in MCT films grown by MBE are apparently tellurium atoms in antistructural positions [32]. Experimental data on the change in the concentration of donor centers in the films MCT growing temperature confirm this assumption. Upon doping with indium in the MCT MBE method, formation of electrically neutral complexes In_2Te_3 does not occur, despite the high tellurium activity [33]. When indium doping is used during film growth of MCT MBE, the concentration of electrons in the films (in the range of $5 \cdot 10^{14}$ to $1.3 \cdot 10^{17}$ cm^{-3}) is directly proportional to the indium concentration, and is not changed by annealing to fill vacancies.

At temperatures above 700°C the As_4 cracking degree reaches saturation [34]. The efficiency of doping by arsenic diatomic molecules is two orders of magnitude higher than by As_4 but activation of arsenic, in any case, requires a high-temperature treatment of MCT films.

12.7 Conclusion

A automated multichamber installation for the growth of HS MBE MCT structures with quality control of the process of growing in real time was created. A set of technological chambers in the installation were determined on the basis of studies of the mechanisms of formation of defects in heterostructures. A MCT growing chamber is equipped with an automatic ellipsometer and molecular sources with ring diffusers. This solves MCT technology problems associated with high demands for homogeneity of composition and control of composition in the process of growing CMT layers.

The equipment allows growth of layers of MCT with a high uniformity of composition across the substrate area, and gives almost unlimited possibilities for modifying the parameters of the layer thickness of MCT, which is necessary for the development of new generations of photodetectors. The technological process is designed based on ideas about the mechanisms of formation and the nature of defects in HgCdTe layers, and allows preparation of the epitaxial structure of MCT with the necessary concentration, carrier mobility, and relaxation time of nonequilibrium photoconductivity. Photoelectric characteristics of HS MBE grown MCT meet the requirements in the manufacture of photosensitive element-based photoconductors and photodiodes.

The quantum well made MBE-based mercury telluride surface orientation (013) found a two-dimensional electron−hole system, consisting of light highly mobile electrons with concentration $N_s = (4-7) \cdot 10^{10}$ cm^{-2} and mobility $\mu_n = (4-6)\ 10^5$ cm^2/V s, and heavier holes with a concentration of $P_s = (0.7-1.6)\ 10^{11}$ cm^{-2} and mobility of $\mu_p = (3-7)\ 10^4$ cm^2/V s. The electron mobility recorded and the observed quantum effects confirm the high quality of the HgCdTe grown.

References

[1] A. Krost, W. Richter, D.R.T. Zahn, et al., Chemical reaction at the ZnSe/GaAs interface detected by Raman spectroscopy, Appl. Phys. Lett. 57 (17) (1990) 1981−1983.

[2] T. Scimeca, Y. Watanabe, F. Maeda, et al., Controlled passivation of GaAs by Se treatment, Appl. Phys. Lett. 62 (14) (1993) 1667−1669.

[3] M.V. Yakushev, V.G. Kesler, L.M. Logvinsky, Yu.G. Sidorov, XPS analysis of the ZnSe/GaAs(112)B heterosystems grown by MBE, Poverhnost 2 (1997) 58−67 (in Russian).

[4] P.K. Larsen, P.L. Dobson (Eds.), Reflection high-energy electron diffraction and reflection electron imaging of surface, NATOASI Ser. B (1988) 188−194.

[5] M.V. Yakushev, Yu.G. Sidorov, L.V. Sokolov, Twinning at the initial stages of MBE growth of A2B6 compounds on GaAs substrates, Poverhnost 10 (1996) 35−46 (in Russian).

[6] F.A. Kuznetsov, Yu.G. Sidorov, I.E. Maronchuk, To the question of quantity description the transport reactions, Fiz. Tverd. Tela 6 (10) (1964) 2981−2983 (in Russian).

[7] C.H. Su, P.-K. Liao, R.F. Brebrick, Partial pressures over the pseudobinary solid solution Hg_{1-x} Cd_x Te(s) for $x = 0.70$ and 0.95 and over four Te-rich ternary melts, J. Electrochem. Soc. 132 (1985) 942−949.

[8] V.S. Varavin, S.A. Dvoretsky, V.I. Liberman, N.N. Mikhailov, Yu.G. Sidorov, The controlled growth of high-quality mercury cadmium telluride, Thin Solid Films 267 (1995) 121−125.

[9] Yu.G. Sidorov, S.A. Dvoretsky, M.V. Yakushev, N.N. Mikhhailov, V.S. Varavin, V.I. Liberman, Pecularities of the MBE growth physics and technology of narrow-gap II-VI compounds, Thin Solid Films 311 (1997) 253–266.

[10] K.K. Svitashev, S.A. Dvoretsky, Yu.G. Sidorov, V.A. Shvets, A.S. Mardezhov, I.E. Nis, et al., The growth of high-quality MCT films by MBE using in situ ellipsometry, Cryst. Res. Technol. 29 (1994) 931–936.

[11] Yu.G. Sidorov, S.A. Dvoretsky, N.N. Mikhhailov, M.V. Yakushev, V.S. Varavin, A.P. Anciferov, Molecular beam epitaxy of compounds $Cd_XHg_{1-X}Te$, Equip. Technol. Optichesky J. 67 (2000) 39–45 (in Russian).

[12] Yu.G. Sidorov, S.A. Dvoretsky, V.S. Varavin, N.N. Mikhhailov, M.V. Yakushev, I.V. Sabinina, Molecular beam epitaxy of solid solutions of cadmium-mercury-tellurium on "alternative" substrates, Fiz. Tech. Poluprovodn. 35 (2001) 1092–1101 (in Russian).

[13] J.F. Nicholas, An Atlas of Models of Crystal Surfaces, Gordon and Breach Science Publishers, New York, NY, 1965.

[14] Yu.G. Galicin, V.G. Mansurov, V.I. Poshevnev, A.S. Terekhov, Surface passivation of GaAs in alcoholic solutions of HCl, Poverhnost 10 (1989) 140–144 (in Russian).

[15] N.N. Mikhailov, V.A. Svets, S.A. Dvoretsky, E.V. Spesivtsev, Yu.G. Sidorov, S.V. Rykhlitski, et al., Ellipsometric control of the growth of nanostructures on the basis of $Cd_xHg_{1-x}Te$, Avtometriya 2 (2003) 71–80 (in Russian).

[16] V.S. Varavin, V.V. Vasiliev, S.A. Dvoretsky, N.N. Mikhailov, V.N. Ovsyuk, Yu.G. Sidorov, et al., HgCdTe epilayers on GaAs: growth and devices, Opto-electronics Rev. 11 (2) (2003) 99–111.

[17] V.A. Svets, S.V. Rykhlitski, E.V. Spesivtsev, N.A. Aulchenko, N.N. Mikhailov, S.A. Dvoretsky, et al., In situ ellipsometry for control of $Hg_{1-x}Cd_xTe$ nanolayer structures and inhomogeneous during MBE growth, Thin Solid Films 455–456 (2004) 688–694.

[18] A.V. Rzanov, K.K. Svitashev, A.S. Mardezhov, V.A. Svets, The control of parameters of the superlattices by the method of ellipsometry in the growing process, Dokl. Akad. Nauk 297 (1987) 604–609 (in Russian).

[19] S. Dvoretsky, N. Mikhailov, Yu Sidorov, V. Shvets, S. Danilov, B. Wittman, et al., Growth of HgTe quantum wells for IR to THz detectors, J. Electron. Mater. 39 (2010) 918–923.

[20] M. Zandian, E. Goo, TEM investigation of defects in arsenic doped layers grown in-situ by MBE, J. Electron. Mater. 30 (2001) 623–627.

[21] D. Chandra, F. Aqariden, J. Frazier, S. Gutzler, T. Orent, H.D. Shih, Isolation and control of voids and void-hillocks during molecular beam epitaxial growth of HgCdTe, J. Electron. Mater. 29 (2000) 887–892.

[22] E.C. Piquette, M. Zandian, D.D. Edwall, J.M. Arias, MBE growth of HgCdTe epilayers with reduced visible defect densities: kinetics considerations and substrate limitations, J. Electron. Mater. 30 (2001) 627–631.

[23] I.V. Sabinina, A.K. Gutakovsky, Preparation of TEM samples from compound semiconductors by chemo-mechanical polishing, Ultramicroscopy 45 (1992) 411–415.

[24] Yu.G. Sidorov, V.S. Varavin, S.A. Dvoretsky, V.I. Liberman, N.N. Mikhailov, I.V. Sabinina, et al., Growth and defect formation in $Cd_xHg_{1-x}Te$ films during molecular beam epitaxy, Growth Cryst. 20 (1996) 35–45.

[25] L. He, Y. Wu, L. Chen, S.L. Wang, M.F. Yu, Y.M. Qiao, et al., Composition control and surface defects of MBE-grown HgCdTe, J. Cryst. Growth 227–228 (2001) 627–631.

[26] I.V. Sabinina, A.K. Gutakovsky, Yu.G. Sidorov, A.V. Latyshev, Nature of V-shaped defects in HgCdTe epilayers grown by molecular beam epitaxy, J. Cryst. Growth 274 (2005) 339–346.

[27] P.S. Wijewarnasuriya, M. Zandian, D.D. Edwall, et al., MBE P-on-n $Hg_{1-x}Cd_xTe$ heterostructure detectors on silicon substrates, J. Electron. Mater. 27 (1998) 546–549.

[28] R.K. Bhan, V. Dhar, P.K. Chaudhury, et al., Comment on "Electrical properties of epitaxially grown CdTe passivation for long-wavelength HgCdTe photodiodes" [Appl. Phys. Lett. 65 (1994) 2725] Appl. Phys. Lett. 68 (1996) 2453−2455.

[29] V.G. Remesnik, A.M. Mischenko, N.N. Mikhailov, Patent RF №2022402, Bulleten izobreteniy №20 (1994).

[30] A. Rogalski, J. Piotrowski, Intrinsic infrared detectors, Prog. Quant. Electron. 12 (2/3) (1988) 87−289.

[31] V.S. Varavin, G.Yu Sidorov, Yu.G. Sidorov, The concentration of vacancies in the metal sublattice of the solid solutions of tellurides of cadmium and mercury, depending on the composition, J. Fiz. Himii 84 (9) (2010) 1605−1612 (in Russian).

[32] V.S. Varavin, S.A. Dvoretsky, N.N. Mikhailov, Yu.G. Sidorov, The donor defects in epitaxial layers of CdHgTe you-for example, by the method of molecular-polar beam epitaxy, Avtometriya 3 (2001) 9−19 (in Russian).

[33] V.S. Varavin, S.A. Dvoretsky, D.G. Ikusov, N.N. Mikhhailov, Yu.G. Sidorov, G.Yu Sidorov, et al., The dependence of electrophysical parameters of the films $Cd_xHg_{1-x}Te$ grown by molecular beam epitaxy, the doping level of indium, Fiz. Tech. Poluprovodn. 42 (6) (2008) 664−667 (in Russian).

[34] G.Yu Sidorov, N.N. Mikhailov, V.S. Varavin, D.G. Ikusov, Yu.G. Sidorov, S.A. Dvoretsky, The study of influence of temperature of arsenic cracking on the efficiency of its incorporation into the CdHgTe film in the process of molecular beam epitaxy, Fiz. Tehn. Poluprovodn. 42 (6) (2008) 668−671 (in Russian).